Int. J. Heat Mass Transfer. Vol. 33, No. 9, pp. 1945–1955, 1990
Printed in Great Britain

0017-9310/90 $3.00 + 0.00

An analysis of the vapor flow and the heat conduction through the liquid-wick and pipe wall in a heat pipe with single or multiple heat sources

MING-MING CHEN† and AMIR FAGHRI
Department of Mechanical and Materials Engineering, Wright State University, Dayton, OH 45435, U.S.A.

(*Received* 3 *July* 1989 *and in final form* 30 *October* 1989)

Abstract—A numerical analysis is presented for the overall performance of heat pipes with single or multiple heat sources. The analysis includes the heat conduction in the wall and liquid-wick regions as well as the compressibility effect of the vapor inside the heat pipe. The two-dimensional elliptic governing equations in conjunction with the thermodynamic equilibrium relation and appropriate boundary conditions are solved numerically. The solutions are in agreement with existing experimental data for the vapor and wall temperatures at both low and high operating temperatures.

INTRODUCTION

THE HEAT pipe is a device which has a very high thermal conductance. It is a closed evacuated tube or chamber of different shapes the inner surfaces of which are lined with a porous capillary wick as shown in Fig. 1. Since 1964, there have been many experimental, analytical, and numerical investigations on heat pipes. The previous related analytical and numerical studies that will be presented here are grouped into the following two categories: (1) analysis of the vapor dynamics, and (2) analysis of the coupled temperature field and vapor dynamics. A summary of the previous theoretical work in both categories is given in Table 1.

Table 1 provides a detailed review for refs. [1–27] of the previous efforts concerning the numerical and theoretical analyses of heat pipes. The table presents information such as one-dimensional vs two-dimensional approximations, elliptic vs parabolic presentations, compressible vs incompressible models as well as the flow and geometric configurations for each reference. Furthermore, some important comments concerning each study are made in the last column of Table 1.

It is the objective of the present paper to include the effects of conjugate heat transfer, vapor compressibility, and viscous dissipation for liquid metal heat pipes by solving the complete conservation of mass, momentum, and energy equations. The present analysis includes the conjugate heat conduction through the wall and the liquid-wick matrix as well as compressibility effect, which is usually neglected but is very important for heat pipes at high operating temperatures. The investigation is also extended to lower temperature heat pipes such as those using water as the working fluid with multiple heat sources. Furthermore, the numerical results are compared with some of the existing experimental data for the wall and vapor temperatures on actual heat pipes rather than simulated heat pipes at both high and low temperatures, which was not done in the previous studies.

MATHEMATICAL FORMULATION

The heat pipe model under consideration is illustrated in Fig. 1, which has three distinct regions in the radial direction (i.e. wall, liquid-wick, and vapor regions) as well as three different types of sections in the axial direction (i.e. evaporator, adiabatic, and condenser). This model solves the two-dimensional conservation of mass, momentum, and energy equations for the heat pipe with single and multiple heat sources under the following assumptions.

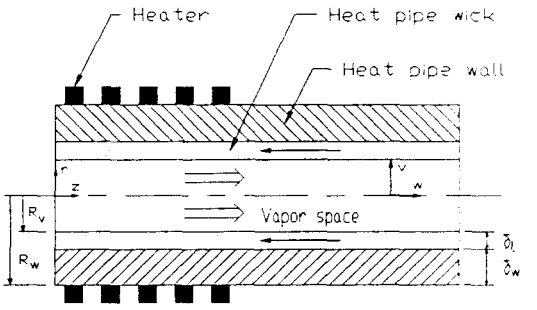

FIG. 1. The multiple evaporator heat pipe and coordinate system.

† Present address: Combustion Engineering, Inc., Wellsville, NY 14895, U.S.A.

NOMENCLATURE

A	surface area of the pipe wall [m^2]
C_p	specific heat at constant pressure [J kg^{-1} K^{-1}]
h_{fg}	latent heat of evaporation [J kg^{-1}]
k	thermal conductivity [W m^{-1} K^{-1}]
L	total length of the pipe [m]
L_a	adiabatic length [m]
L_c	condenser length [m]
L_e	evaporator length [m]
M	Mach number
$\dot{m}$	mass flux [kg m^{-2} s^{-1}]
P	pressure of the fluid [N m^{-2}]
P_0	datum pressure at the end cap of the evaporator at the liquid–vapor interface [N m^{-2}]
Q	total heat input rate at the outer pipe wall in the evaporator [W]
q	heat flux [W m^{-2}]
R_v	vapor space radius [m]
R_w	outer pipe wall radius [m]
r	radial coordinate [m]
T	temperature [K]
T_0	temperature of the evaporator end cap at the liquid–vapor interface [K]
v	radial velocity [m s^{-1}]
w	axial velocity [m s^{-1}]
z	axial coordinate [m].

Greek symbols

δ	wall or liquid-wick thickness [m]
ε	wick porosity
μ	dynamic viscosity of the fluid [kg m^{-1} s^{-1}]
ρ	density of the fluid [kg m^{-3}]
ϕ	viscous dissipation term in equation (4).

Subscripts

a	adiabatic
c	condenser
e	evaporator
eff	effective
i	vapor–liquid interface
l	liquid
lw	liquid-wick
o	variable at the outer pipe wall
s	solid
v	vapor
w	wall
0	properties corresponding to T_0.

(a) The compressible vapor flow is laminar and steady.

(b) The heat transfer through the liquid-wick is modeled as purely conduction with an effective thermal conductivity.

(c) The properties of the liquid and the solid in the wall and wick regions are constant with the vapor density following the perfect gas law in the vapor region. The vapor density and pressure are the only major temperature-dependent properties for sodium as the working fluid. The perfect gas law assumption accounts for this variation.

(d) Both evaporation and condensation are considered to occur at the inner radius of the porous medium.

(e) At the vapor–liquid interface, the vapor is at its thermodynamic equilibrium temperature corresponding to the local saturation vapor pressure.

(f) At the liquid-wick/vapor and wall/liquid-wick interfaces, the harmonic mean of the thermal conductivity is used in the energy equation.

(g) The vapor flow is axisymmetric.

The conservation of mass, momentum, and energy equations for the compressible flow analysis including the viscous dissipation terms for the case of constant viscosity and thermal conductivity are

$$\frac{\partial}{\partial z}(\rho w)+\frac{1}{r}\frac{\partial}{\partial r}(\rho r v)=0 \tag{1}$$

$$\rho\left(v\frac{\partial v}{\partial r}+w\frac{\partial v}{\partial z}\right)=-\frac{\partial P}{\partial r}+\mu\left[\frac{4}{3r}\frac{\partial}{\partial r}\left(r\frac{\partial v}{\partial r}\right)-\frac{1}{3}\frac{v}{r^2}+\frac{1}{3}\frac{\partial^2 w}{\partial z\,\partial r}+\left\{\frac{\partial^2 v}{\partial z^2}\right\}\right] \tag{2}$$

$$\rho\left(v\frac{\partial w}{\partial r}+w\frac{\partial w}{\partial z}\right)=-\frac{\partial P}{\partial z}+\mu\left[\frac{1}{r}\frac{\partial}{\partial r}\left(r\frac{\partial w}{\partial r}\right)+\frac{1}{r}\frac{\partial}{\partial r}\left(r\frac{\partial v}{\partial z}\right)-\frac{2}{3}\frac{\partial}{\partial z}\left(\frac{1}{r}\frac{\partial}{\partial r}(rv)\right)+\left\{\frac{4}{3}\frac{\partial^2 w}{\partial z^2}\right\}\right] \tag{3}$$

$$\rho C_p\left(v\frac{\partial T}{\partial r}+w\frac{\partial T}{\partial z}\right)=k\left[\frac{1}{r}\frac{\partial}{\partial r}\left(r\frac{\partial T}{\partial r}\right)+\left\{\frac{\partial^2 T}{\partial z^2}\right\}\right]+v\frac{\partial P}{\partial r}+w\frac{\partial P}{\partial z}+\mu\phi \tag{4}$$

where

$$\phi=2\left[\left(\frac{\partial v}{\partial r}\right)^2+\left(\frac{v}{r}\right)^2+\left(\frac{\partial w}{\partial z}\right)^2+\frac{1}{2}\left(\frac{\partial v}{\partial z}+\frac{\partial w}{\partial r}\right)^2-\frac{1}{3}(\nabla\cdot\mathbf{v})^2\right]$$

$$\nabla\cdot\mathbf{v}=\frac{1}{r}\frac{\partial}{\partial r}(rv)+\frac{\partial w}{\partial z}.$$

The convective terms and the viscous dissipation, ϕ, are included in the vapor analysis. It should be mentioned here that in equations (2)–(4), the terms in

Table 1. Related numerical or analytical work on heat pipes

References	Analysis	1-D or 2-D (vapor)	Equations solved	Elliptic or parabolic	Compressible or incompressible	Geometry	Flow type	Comments
Cotter (1965) [1]	Analytical No wall	1-D	Mass + momentum	Parabolic	Incompressible	Cylinder	Laminar, steady	Analytical expressions for pressure drop with limiting cases $Re_r \ll 1$ and $Re_r \gg 1$
Busse (1967) [2]	Analytical No wall	1-D	Mass + momentum	Parabolic	Incompressible	Cylinder	Laminar, steady	Analytical expressions for vapor pressure drop were obtained
Levy (1968) [3]	Analytical No wall	1-D	Mass + momentum + energy	N/A	Compressible (equilibrium two-phase)	Cylinder	Laminar, steady	Numerical results for pressure, velocity and sonic heat transfer rate were presented for high temperature liquid metal heat pipes
Bankston and Smith (1973) [4]	Numerical and analytical (slow motion) No wall	2-D	Mass + momentum	Elliptic	Incompressible	Cylinder	Laminar, steady	The governing equations in terms of stream function and vorticity were solved numerically. Analytical results were obtained for low Reynolds number cases
Rohani and Tien (1973) [5]	Numerical (finite difference) No wall	2-D	Mass + momentum + energy + species	Elliptic	Compressible (perfect gas law)	Cylinder	Laminar, steady	The stream function and vorticity type of equations were solved. The effect of gas loaded heat pipe was analyzed
Busse (1973) [6]	Analytical No wall	2-D	Mass + momentum	Parabolic	Compressible	Cylinder	Laminar, steady	An approximate methodology was developed. Ultimate limits of heat pipes were discussed and analyzed
Tien and Rohani (1974) [7]	Numerical (finite difference) No wall	2-D	Mass + momentum + energy	Elliptic	Compressible (perfect gas law)	Cylinder	Laminar, steady	Elliptic energy equation was solved simultaneously with the stream function and vorticity equations
Kadaner and Rassadkin (1975) [8]	Analytical No wall	1-D	Mass + momentum	Parabolic	Incompressible	Cylinder	Laminar, steady	Pressure drop and friction coefficient vs Reynolds number and axial distance were presented
Bystrov and Popov (1976) [9]	Analytical No wall	1-D	Mass + momentum	N/A	Compressible (equilibrium two-phase)	Cylinder	Laminar, steady	The pressure profile and the sonic limit in terms of temperature were presented for high temperature liquid metal heat pipes
Oijen and Hoogendoorn (1979) [10]	Numerical (finite difference) No wall	2-D	Mass + momentum	Elliptic	Incompressible	Rectangle	Laminar, steady	Comparison was made with flat simulated heat pipe
Bystrov and Mikhailov (1982) [11]	Analytical No wall	1-D	Mass + momentum	Parabolic	Incompressible	Cylindrical condenser	Laminar, steady	Parametric method was used
Busse and Prenger (1984) [12]	Analytical No wall	1-D	Mass + momentum	Parabolic	Compressible (perfect isothermal gas)	Cylinder	Laminar, steady	A generalized code was developed for gas dynamics. The isothermal perfect gas was chosen for analyzing heat pipes with organic working fluids

Table 1 (*continued*)

References	Analysis	1-D or 2-D (vapor)	Equations solved	Elliptic or parabolic	Compressible or incompressible	Geometry	Flow type	Comments
Faghri (1986) [13]	Numerical (finite difference) No wall	2-D	Mass + momentum	Parabolic	Incompressible	Annulus	Laminar, steady	Numerical analysis for annular heat pipe
Narayana (1986) [14]	Numerical (finite difference) No wall	2-D	Mass + momentum	Parabolic	Incompressible	Cylinder	Laminar, steady	The results for pressure drop were presented for $Re_r = 2 \sim -5.0$
Colwell *et al.* (1987) [15]	Analytical (vapor) + finite element (wall + wick)	1-D	Mass + momentum + energy	N/A	Compressible (equilibrium two-phase)	Rectangle	Laminar, steady	Analysis was related to the start-up of a frozen heat pipe
Bianchi (1987) [16]	Numerical (finite element) No wall	2-D	Mass + momentum + energy	Elliptic	Incompressible	Cylinder	Laminar, steady	Comparison with experimental data using water as working fluid. The viscous dissipation is included in the energy equation
Ismail *et al.* (1987) [17]	Numerical (finite difference) No wall	2-D	Mass + momentum + energy	Elliptic	Incompressible	Cylinder	Laminar, steady	No discussion of the solution procedure is given. The governing equation is given with some general trends of the results
Busse (1987) [18]	Analytical No wall	2-D	Mass + momentum	Parabolic	Compressible (perfect isothermal gas)	Cylinder	Laminar, steady	A logical criterion for determining the flow type was presented for the heat pipe condenser
Faghri and Parvani (1988) [19]	Numerical (finite difference) No wall	2-D	Mass + momentum	Elliptic and parabolic	Incompressible	Annulus	Laminar, steady	Comparison between elliptic and parabolic solutions for $Re_r \leqslant 1000$ using water as working fluid
Faghri (1989) [20]	Analytical + numerical No wall	1-D & 2-D	Mass + momentum + energy	Elliptic and parabolic	Incompressible (2-D) Compressible (1-D)	Annulus and cylinder	Laminar, steady	Analytical expressions for pressure drop at each section of the heat pipe were given both for conventional and annular heat pipes. The results for 1-D were in good agreement with 2-D model

Issacci *et al.* (1988) [21]	Numerical (finite difference) No wall	2-D	Mass + momentum + energy	Elliptic	Compressible (perfect gas law)	Rectangle	Laminar, transient	Only velocity profile was presented. The numerical results were presented at low temperature
Bowman and Hitchcock (1988) [22]	Numerical (finite difference) No wall	2-D	Mass + momentum	Elliptic	Compressible (perfect gas law)	Cylinder	Laminar, turbulent and transient	Comparison was made with experimental data of simulated heat pipe using air as a working fluid
Seo and El-Genk (1988) [23]	Numerical (finite difference) With wall	1-D	Mass + momentum + energy	N/A	Compressible (perfect gas law)	Cylinder	Laminar, steady	The effect of porosity in the liquid wick is neglected. The energy due to mass injection and suction to the vapor region is also neglected
Busse and Lochrke (1989) [24]	Analytical + numerical No wall	2-D	Mass + momentum	Parabolic	Compressible (perfect isothermal gas)	Cylinder	Laminar, steady	Emphasis on flow reversal and pressure recovery. An empirical wall-friction parameter was also obtained for the prediction of subsonic turbulent pressure recovery
Jang *et al.* (1989) [25]	Numerical No wall	1-D	Mass + momentum + energy	N/A	Compressible (perfect gas law)	Cylinder	Laminar, turbulent and transient	The transient behavior of vapor flow under subsonic, sonic and supersonic speeds is successfully predicted
Jang *et al.* (1989) [26]	Numerical With wall and wick	1-D	Mass + momentum + energy	N/A	Compressible (perfect gas law)	Cylinder	Laminar, turbulent and transient	Analysis related to the start-up from frozen state. The wall and wick are modelled as two-dimensional
Cao and Faghri (1990) [27]	Numerical (finite difference) With wall	2-D	Mass + momentum + energy	Elliptic	Compressible (perfect gas law)	Cylinder	Laminar, transient	A complete transient model analysis for high Mach numbers for high temperature heat pipes with a pulsed heat input
Chen and Faghri [present]	Numerical (finite difference) With wall	2-D	Mass + momentum + energy	Elliptic	Compressible (perfect gas law)	Cylinder	Laminar, steady	The energy due to mass injection and suction to the vapor region is included. The numerical results are compared with both low and high temperature experimental data

braces { } are associated with axial diffusion terms. These terms are neglected in the partially-parabolic version but are included in the elliptic version. In the wall and liquid-wick regions, only heat conduction is considered and therefore the convective terms were neglected. The relation for the liquid–vapor interface was analyzed [27] and justification is given by simple numerical calculations for modeling the wick structure as a conduction problem. This does not mean that the liquid flow in the porous wick is not important. In fact, the liquid flow in the porous wick is very important to determine the capillary limit of heat pipes. It is assumed that the wick structure is designed such that it has enough capillary force to drive condensate to the evaporator section. The perfect gas law is employed to account for the compressibility of the vapor. The thermal conductivity k of the wall is different from that of the liquid-wick structure. The equations for the effective thermal conductivity proposed by Dunn and Reay [28] were used for the liquid-saturated screen wick, sintered powder wick as well as the concentric annulus wick. The wick porosity for screen wicks was given by Chang [29].

Boundary condition specifications are needed at the outer pipe, wall/liquid-wick interface, liquid-wick/vapor interface as well as both ends of the heat pipe. This information is provided in Table 2. It should be noted that in addition to a mass and energy balance at the liquid-wick/vapor interface, the Clapeyron equation is used to define thermodynamic equilibrium.

NUMERICAL METHODOLOGY

The heat pipe problem is solved as a convection–conduction problem throughout the entire domain by solving one generalized energy equation with different thermal diffusion coefficients. The velocity in the solid wall and the liquid-wick matrix is specified to be zero so that the analysis in these two regions becomes purely a conduction problem. Since the liquid velocity in the porous medium is much slower compared to the vapor flow, the zero velocity boundary condition at the liquid–vapor interface and neglecting the convective term in the energy equation of the liquid-wick region should not cause a large accuracy problem. The validity of the results will be checked with experimental data.

The numerical procedure employs the finite-difference iterative method of solution developed by Spalding [30]. The elliptic solutions of the mass, momentum, and energy conservation equations with the boundary conditions given in Table 2 were obtained. The partially parabolic solution was also obtained by neglecting the axial diffusion terms in the momentum and energy equations. The solution procedure is based on a line-by-line iteration method in the axial direction and the Jacobi point-by-point procedure in the radial direction. The 'SIMPLEST' [31] method is employed for the momentum equations, in which the finite-domain coefficients contain only diffusion contributions, and where the convective terms are added to the linearized source term of the equations.

Since there is a change of phase at the liquid–vapor interface, the energy equation is no longer continuous due to the latent heat of evaporation or condensation. To make an energy balance, we can include the term $\dot{m}h_{fg}$ as a heat sink at the liquid–vapor interface in the evaporator and as a heat source at the interface in the condenser section. Therefore, the sign of q_i in the evaporator should be negative and positive in the condenser.

The governing equation of the vapor flow is first

Table 2. Boundary conditions for heat pipe analysis

	Evaporator ($0 \leqslant z \leqslant L_e$)	Adiabatic ($L_e \leqslant z \leqslant L_e+L_a$)	Condenser ($L_e+L_a \leqslant z \leqslant L$)
Outer pipe wall ($r = R_w$)	$-k_w \frac{\partial T_w}{\partial r} = q_{o,e}$	$\frac{\partial T_w}{\partial r} = 0$	$-k_w \frac{\partial T_w}{\partial r} = q_{o,e} \frac{A_e}{A_c}$
Wall and liquid-wick interface ($r = R_v+\delta_1$)	$T_{lw} = T_w, \quad k_w \frac{\partial T_w}{\partial r} = k_{eff} \frac{\partial T_{lw}}{\partial r}$		
Liquid–vapor interface ($r = R_v$)	$w_v = 0, \quad v_i = \frac{\dot{m}}{\rho_v}, \quad q_i = \dot{m}h_{fg} = k_v \frac{\partial T_v}{\partial r} - k_{eff} \frac{\partial T_{lw}}{\partial r}$		
	$T_i = \frac{1}{\frac{1}{T_0} - \frac{R}{h_{fg}} \ln \frac{P_v}{P_0}}$		
Centerline of the pipe ($r = 0$)	$\frac{\partial w_v}{\partial r} = 0, \quad v_v = 0, \quad \frac{\partial T_v}{\partial r} = 0$		
Both ends of the pipe ($z = 0, L$)	$w = v = \frac{\partial T}{\partial z} = 0$		

Table 3. Experimental heat pipe specifications and properties

	Case No. 1	2	3	4
References	Ivanovskii *et al.* [32]	Ivanovskii *et al.* [32]	Kemme [33]	Gernert [34]
Working fluid	Sodium	Sodium	Sodium	Water
P_0 (N m^{-2})	1300	2476	12460	85710
T_0 (°C)	545	583	692	94
L_e (m)	0.1	0.1	0.143	0.1, 0.1
L_a (m)	0.05	0.05	0.06	0.4, 0.3
L_c (m)	0.35	0.55	1.08	0.6
Vapor channel radius (mm)	7.0	7.0	5.7	11.0
Wick type	Ring-shaped gap (screen mesh)	Ring-shaped gap (screen mesh)	Screen mesh	Sintered powder
Mesh number (per in.^{2})	Not reported	Not reported	400	325
Wick thickness, δ_1 (mm)	0.5	0.5	0.15	0.76
Wall material	Stainless steel (assumed)	Stainless steel (assumed)	Stainless steel	Copper
Wall thickness, δ_w (mm)	1.0 (assumed)	1.0 (assumed)	0.9	1.6
Total heat input, Q (W)	560	1000	6400	200 + 800
Grid number (radial × axial)	35 × 50	35 × 70	35 × 50	40 × 60
k_{eff} (W m^{-1} K^{-1})	66.18	66.18	45.45	240.2
ε	0.33	0.33	0.74	0.30

solved by assuming that the heat flux is uniform at the liquid–vapor interface based on the total heat input at the outer wall. The rate of evaporation, condensation and the velocity are then calculated by $\dot{m} = q_i/h_{fg}$ and $v_i = \dot{m}/\rho_v$. These values are used in the vapor mass and momentum conservation equations. Once a converging solution is obtained after a few iterations, a new q_i is calculated by an exact energy balance and this method is used for further iterations. At the same time, the thermodynamic equilibrium is checked and corrected during each iteration. The algorithm continues iterating until fully converged results are obtained. The pressure at the liquid–vapor interface at the end of the evaporator, P_0, is taken as the datum pressure and does not change. The corresponding saturation temperature T_0 is assumed to be the initial temperature for the numerical computations.

The accuracy of the numerical solution is checked with experimental data and the convergence is assured in two ways.

(1) The sum of the absolute value of the residuals should decrease as the sweep number increases.

(2) The spot value should approach a constant value as the sweep number increases.

As a common approach, a coarse grid size is first chosen to test the program and a fine grid spacing is employed for the final solution. A uniform grid size is used for the axial direction and three different uniform grid sizes are used for the vapor, liquid-wick, and wall regions. For the numerical results presented for this paper, the grid sizes for the cases presented are mentioned in Table 3.

MODEL VERIFICATION VS EXPERIMENTAL DATA

To verify the numerical predictions, the results are compared with four cases of existing experimental data reported by several investigators as listed in Table 3. The numerical model was first compared with the experimental data reported by Ivanovskii *et al.* [32] for a cylindrical sodium heat pipe (Case 1). The heat pipe was provided with a compound wick of the type with a ring-shaped gap for the flow of liquid. The method of measuring the temperature distribution was to place a movable micro-thermocouple directly in the vapor channel. The thermocouple was provided with a special capillary device to keep it wetted by the condensate, so the temperature readings correspond to the saturation temperature which matches the numerical model at the interface.

For the numerical computation, a constant heat flux with a total heat input of 560 W is specified at the outer wall of the evaporator. The pipe wall is assumed to be made of stainless steel and have a thickness of $\delta_w = 1$ mm. At the condenser, a constant heat flux based on the total heat input at the outer wall of the evaporator section is also specified. Figure 2 gives a

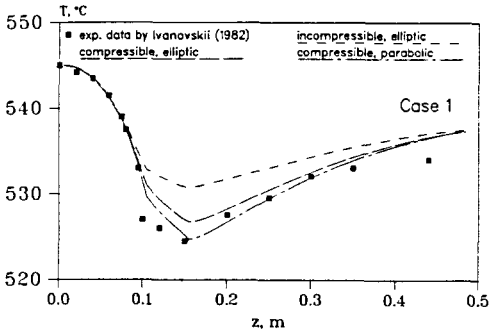

FIG. 2. The axial interface temperature profile along the sodium heat pipe with $Q = 560$ W, $R_v = 0.007$ m, $L_e = 0.1$ m, $L_a = 0.05$ m, $L_c = 0.35$ m, $k_l = 66.2$ W m^{-2} K^{-1}, $k_s = 19.0$ W m^{-2} K^{-1}, $\delta_l = 0.0005$ m, $\delta_w = 0.001$ m.

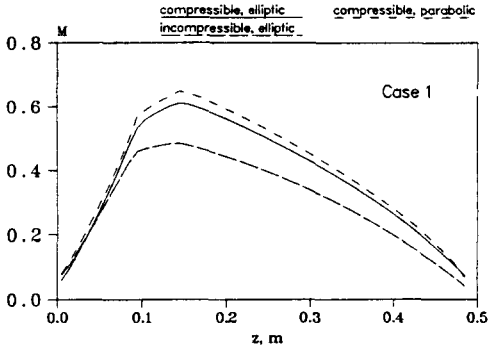

FIG. 4. The axial Mach number along the centerline of the sodium heat pipe with $Q = 560$ W, $R_v = 0.007$ m, $L_e = 0.1$ m, $L_a = 0.05$ m, $L_c = 0.35$ m, $k_l = 66.2$ W m^{-2} K^{-1}, $k_s = 19.0$ W m^{-2} K^{-1}, $\delta_l = 0.0005$ m, $\delta_w = 0.001$ m.

comparison between the numerical results and the experimental data for the vapor saturation temperature along the heat pipe for Case 1. As the results show, the present compressible elliptic and partially parabolic models give accurate predictions of the temperature profile compared with the experimental data with a maximum deviation of 3°C. According to Ivanovskii *et al.* [32], the experimental data for the heat transfer rate were measured with an accuracy of 6–10%, so the deviations of the present compressible models are within the range of experimental accuracy. For the incompressible model, however, there is a maximum deviation of about 6°C at the inlet of the condenser section. Therefore, the effect of the compressibility of the vapor needs to be included in the analysis.

Figure 3 shows the variation of the pressure along the liquid–vapor interface for Case 1. The pressure drop reaches its maximum value at the exit of the adiabatic section and then recovers about 55% in the condenser. Since the Clapeyron equation is the link between the temperature and the pressure at the liquid–vapor interface, the pressure profile is similar to the saturated temperature distribution. The trend of the pressure profile is also in agreement with the numerical results obtained by Tien and Rohani [7].

Figure 4 shows the variation of the Mach number along the centerline of the pipe with a maximum value of $M = 0.6$ at the inlet of the condenser for the compressible elliptic model. The trend is generally in agreement with the results obtained for a cylindrical heat pipe [3] and for an annular heat pipe [20] with a one-dimensional compressible model.

Figure 5 shows the numerical results for the axial temperature corresponding to Case 2 of the experimental data by Ivanovskii *et al.* [32]. For this case, the heat input was $Q = 1000$ W. Since the thickness of the wall and the type of materials were not mentioned in the reference, numerical calculations were made with two different thermal conductivities and thicknesses for the pipe wall which are believed to be commonly used by heat pipe manufacturers. The results of the compressible and incompressible models for the vapor flow are presented vs the experimental data for the interface temperature in Fig. 5. It shows that both models give a very good prediction in the evaporator region, but the incompressible model overpredicts the data in the adiabatic and condenser regions while the

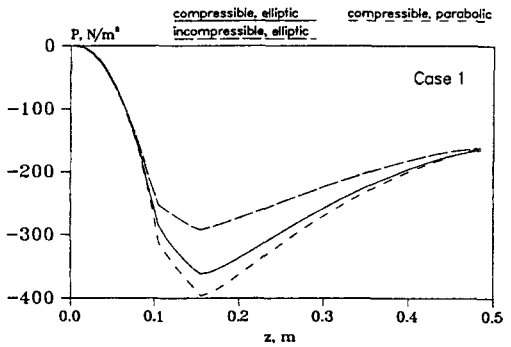

FIG. 3. The axial interface temperature profile along the sodium heat pipe with $Q = 560$ W, $R_v = 0.007$ m, $L_e = 0.1$ m, $L_a = 0.05$ m, $L_c = 0.35$ m, $k_l = 66.2$ W m^{-2} K^{-1}, $k_s = 19.0$ W m^{-2} K^{-1}, $\delta_l = 0.0005$ m, $\delta_w = 0.001$ m.

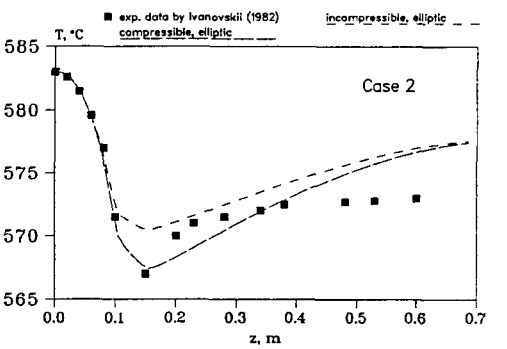

FIG. 5. The axial interface temperature profile along the sodium heat pipe with $Q = 1000$ W, $R_v = 0.007$ m, $L_e = 0.1$ m, $L_a = 0.05$ m, $L_c = 0.55$ m, $k_l = 66.2$ W m^{-2} K^{-1}, $k_s = 19.0$ W m^{-2} K^{-1}, $\delta_l = 0.0005$ m, $\delta_w = 0.001$ m.

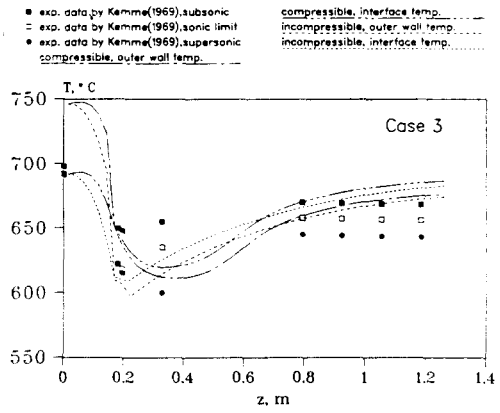

FIG. 6. The axial interface temperature profile along the sodium heat pipe with $Q = 6.4$ kW, $R_v = 0.0057$ m, $L_e = 0.143$ m, $L_a = 0.06$ m, $L_c = 1.08$ m, $k_l = 59.5$ W m^{-2} K^{-1}, $k_w = 19.0$ W m^{-2} K^{-1}, $\delta_l = 0.00015$ m, $\delta_w = 0.0009$ m.

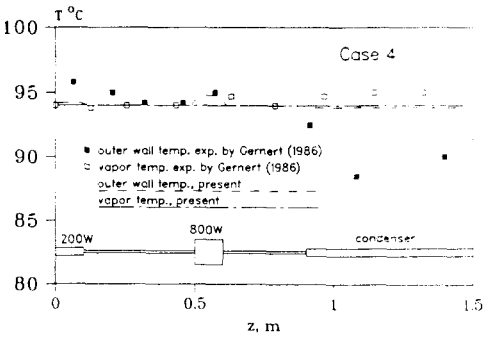

FIG. 7. The axial temperature profile along the water heat pipe with multiple heat sources.

compressible model underpredicts the data at the start of the condenser region and overpredicts it near the end. In general, the compressible model gives a better prediction.

Figure 6 shows the numerical results for the axial temperature variation which corresponds to Case 3 of the experimental data by Kemme [33]. The heat pipe was about 1.3 m long and 5.7 mm i.d. with a screen wrap wick of thickness $\delta_l = 0.15$ mm and stainless steel wall of thickness $\delta_w = 0.9$ mm. Heat was added to the evaporator section of the heat pipe with an induction coil while it was removed from the condenser section by conduction through a gas gap to a water calorimeter. For this case, three different sets of experimental data of the outer wall temperature were obtained for subsonic, sonic and supersonic vapor flow in the sodium heat pipe. During the experiment, the heat input was fixed at 6.4 kW and the working temperature was decreased by changing the cooling conditions so the choked condition could be reached.

For the present numerical analysis, the temperature at the end cap of the evaporator is fixed at the experimental value of 692°C and one steady state solution is obtained with a Mach number of $M = 1.0$ at the exit of the adiabatic section of the compressible model. Figure 6 presents the experimental data of the wall temperature and the numerical solutions of the compressible and incompressible models. It can be seen that the present results of both models are generally in agreement with Kemme's data for the sonic limit case except that the condenser wall temperature is higher than the experimental data. This is probably because the condenser cooling may affect the accuracy of the thermocouple reading and make the reading lower than the actual value. However, according to the comparison it seems that the present model can still predict the general trend of the heat pipe performance even if the Mach number of the vapor flow is high.

To further check the validity of the present numerical analysis, the numerical code was also modified to predict the performance of a water heat pipe with multiple heat sources. The results were compared with the experimental data obtained by Gernert [34]. The experimental heat pipe under consideration had two evaporators and one condenser as illustrated in Fig. 7. The heat was provided at the evaporator by two electric heater blocks. The condenser section was fitted with a water-cooled calorimeter. The heat pipe had a sintered powder wick and the effective thermal conductivity was calculated from Dunn and Reay [28]. A multipoint thermocouple was installed along the centerline of the vapor space to measure the variations of the vapor temperature. To measure the outer wall temperature, the outer wall of the evaporator and condenser sections were grooved and thermocouples were soldered into the grooves in the pipe wall. According to the experimental conditions, two constant heat fluxes with heat inputs of 200 and 800 W were specified at the two evaporator sections. For the condenser section, a constant heat flux based on the total heat input is also specified as a boundary condition for the numerical computation.

Figure 7 shows the numerical results and the experimental data for the outer wall and the vapor temperature of the water heat pipe with multiple heat sources for Case 4. It can be seen that the present model gives a very uniform vapor temperature and a very small outer wall temperature variation. The measured vapor temperature is also fairly uniform with less than a 1°C temperature difference along the pipe. The use of copper as the wall and wick materials and the sintered powder wick gives a very good thermal conductivity, thus the radial temperature drop is very small through the wall and liquid-wick.

For the outer wall temperature, two experimental data points found in the adiabatic section and one in the 800 W evaporator are fairly close to the numerical solutions, but the temperature readings in the condenser section are almost 6°C below the present predictions. Since the length of the condenser is much longer than that of the total length of the evaporator, the heat flux through the pipe wall of the condenser is smaller than that in the evaporator with $Q =$

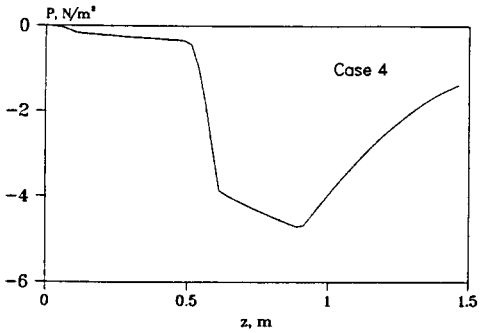

FIG. 8. The axial pressure profile along the vapor–liquid interface of the water heat pipe with multiple heat sources.

800 W. Thus, it is expected to have a smaller temperature gradient through the pipe wall in the condenser section. It seems the measurements were not very accurate in the condenser section probably due to the influence of the cooling water on the thermocouple readings which resulted in the readings being lower than expected. Usually, it is very difficult to measure the condenser and evaporator wall temperatures because the cooling water may lower the actual measurement while the heaters may cause higher temperature readings. Furthermore, the accuracy of the thermocouple reading may also cause problems when the readings differ by only 1 or 2°C.

Figure 8 shows the pressure variation along the vapor–liquid interface of the water heat pipe for Case 4. A very small pressure drop is noticed along the 200 W evaporator and the adjacent adiabatic section, but in the 800 W evaporator the additional amount of heat flux causes more liquid to be evaporated into the vapor channel, thus leading to a significant pressure drop along this section. In the condenser section about 80% of the pressure drop is recovered. As the results show, the total pressure drop is very small which means that a very uniform vapor temperature profile can be obtained. The uniform temperature profile is a result of the thermodynamic equilibrium between the pressure and temperature at the liquid–vapor interface coupled with the fact that water has a high static vapor pressure and vapor density under normal working conditions. The phenomena observed here are in agreement with what is observed for a heat pipe with one evaporator section. It is believed that the present model can predict the general performance of heat pipes with multiple heat sources and will also provide a guideline for further experiments in this respect.

CONCLUSIONS

The performance of heat pipes has been studied numerically and the results show a fairly good agreement compared with the existing experimental data at both low and high operating temperatures. It is also believed that the present model can predict the general performance of heat pipes with single or multiple heat sources. Furthermore, the vapor compressibility should be considered for the prediction of the sodium heat pipe temperature profile when the Mach number is greater than $M = 0.3$. For the heat pipe using water as the working fluid, the vapor temperature along the heat pipe is almost uniform. This is due to a very small pressure drop along the pipe compared with the static vapor pressure and also the thermodynamic equilibrium between the pressure and temperature at the liquid–vapor interface.

Acknowledgement—Funding for this work was provided by a joint effort of the NASA Lewis Research Center and the Thermal Energy Group of the Aero Propulsion Laboratory of the U.S. Air Force under contract F33615-88-C-2820.

REFERENCES

1. T. P. Cotter, Theory of heat pipes, Report LA-3246-MS (1965).
2. C. A. Busse, Pressure drop in the vapor phase of long heat pipes, Thermionic Conversion Specialist Conf., Palo Alto, California, pp. 391–398 (1967).
3. E. K. Levy, Theoretical investigation of heat pipes operating at low vapor pressure, *J. Engng Ind.* **90**, 547–552 (1968).
4. C. A. Bankston and H. J. Smith, Vapor flow in cylindrical heat pipes, *ASME J. Heat Transfer* **95**, 371–376 (1973).
5. A. R. Rohani and C. L. Tien, Steady two-dimensional heat and mass-transfer in the vapor–gas region of a gas-loaded heat pipe, *ASME J. Heat Transfer* **95**, 377–382 (1973).
6. C. A. Busse, Theory of the ultimate heat transfer limit of cylindrical heat pipes, *Int. J. Heat Mass Transfer* **16**, 169–186 (1973).
7. C. L. Tien and A. R. Rohani, Analysis of the effect of vapor-pressure drop on heat pipe performance, *Int. J. Heat Mass Transfer* **17**, 61–67 (1974).
8. Ya. S. Kadaner and Yu. P. Rassadkin, Laminar vapor flow in a heat pipe, *Inzh.-fiz. Zh.* **28**, 208–216 (1975).
9. P. I. Bystrov and A. N. Popov, A study of the characteristics of heat pipes with liquid metal working fluids in low temperature regimes, *Teplofiz. Vys. Temp.* (*USSR*) **14**, 629–637 (1976).
10. H. Van Oijen and C. J. Hoogendoorn, Vapor flow calculations in a flat-plate heat pipe, *AIAA J.* **17**, 1251–1259 (1979).
11. P. I. Bystrov and V. S. Mikhailov, Laminar flow of vapor flux in the condensation region of the heat tubes, *Teplofiz. Vys. Temp.* (*USSR*) **20**, 311–316 (1982).
12. C. A. Busse and F. C. Prenger, Numerical analysis of the vapor flow in cylindrical heat pipes, *Res. Dev. Heat Pipe Technol.*, pp. 214–219 (1984).
13. A. Faghri, Vapor flow analysis in a double-walled concentric heat pipe, *Numer. Heat Transfer* **10**, 583–595 (1986).
14. K. B. Narayana, Vapor flow characteristics of slender cylindrical heat pipes—a numerical approach, *Numer. Heat Transfer* **10**, 79–93 (1986).
15. G. T. Colwell, J. H. Jang and C. J. Camarda, Modeling of startup from the frozen state, *6th Int. Heat Pipe Conf.*, Vol. 1, pp. 165–170 (1987).
16. A. M. Bianchi, Finite element method application to the vapor flow study in a cylindrical wick heat pipe, *6th Int. Heat Pipe Conf.*, Vol. 1, pp. 86–92 (1987).
17. K. A. R. Ismail, M. A. Zanardi and C. Y. Liu, Two-dimensional analysis of flow and heat transfer in a porous heat pipe, *6th Int. Heat Pipe Conf.*, pp. 164–167 (1987).

18. C. A. Busse, On the development of laminar flows with mass injection and extraction, *J. Fluids Engng* **109**, 448–452 (1987).
19. A Faghri and S. Parvani, Numerical analysis of laminar flow in a double-walled annular heat pipe, *J. Thermophys.* **2**, 165–171 (1988).
20. A. Faghri, Performance characteristics of a concentric annular heat pipe, Part II. Vapor flow analysis, *ASME J. Heat Transfer* **111**, 851–857 (1989).
21. F. Issacci, I. Catton, A. Heiss and N. M. Ghoniem, Analysis of heat pipe vapor dynamics, *Proc. 24th ASME National Heat Transfer Conf.*, Vol. 1, pp. 361–366 (1988).
22. J. Bowman and J. Hitchcock, Transient compressible heat pipe vapor dynamics, *Proc. 24th ASME National Heat Transfer Conf.*, Vol. 1, pp. 329–338 (1988).
23. J. T. Seo and M. S. El-Genk, A transient model for liquid metal heat pipes, 5th Symp. on Space Nuclear Power Systems (1988).
24. C. A. Busse and R. I. Loehrke, Subsonic pressure recovery in cylindrical condensers, *ASME J. Heat Transfer* **111**, 533–537 (1989).
25. J. H. Jang, A. Faghri and W. S. Chang, Analysis of the transient compressible vapor flow in heat pipes, *Proc. 1989 ASME National Heat Transfer Conf.*, Philadelphia, HTD-Vol. 110, pp. 113–120 (1989).
26. J. H. Jang, A. Faghri, W. S. Chang and E. T. Mahefkey, Mathematical modeling and analysis of heat pipe start-up from the frozen state, *Proc. 1989 ASME Annual Conf.*, San Francisco, HTD-Vol. 114, pp. 11–20 (1989). Also to appear in *ASME J. Heat Transfer*.
27. Y. Cao and A. Faghri, A transient two-dimensional compressible analysis for high temperature heat pipes with a pulsed heat input, to appear in *Numer. Heat Transfer* (1990).
28. P. D. Dunn and D. A. Reay, *Heat Pipes* (3rd Edn). Pergamon Press, Oxford (1982).
29. W. S. Chang, Effective thermal conductivity of wire screens. In *Fundamentals of Conduction and Recent Developments in Contact Resistance*, HTD 69, pp. 64–75 (1987).
30. D. B. Spalding, Mathematical modeling of fluid-mechanics, heat transfer and chemical-reaction processes, a lecture course, CFDU Report HTS/80/1, Imperial College, London (1980).
31. D. B. Spalding, A general purpose computer program for multi-dimensional one- and two-phase flow, *J. Math. Comput. Simul.* **XXIII**, 267–276 (1981).
32. M. N. Ivanovskii, V. P. Sorokin and I. V. Yagodkin, *The Physical Principles of Heat Pipes*, Chap. 2. Oxford University Press, Oxford (1982).
33. J. E. Kemme, Ultimate heat-pipe performance, *IEEE Trans. Electron. Devices* **ED16**, 717–723 (1969).
34. N. J. Gernert, Analysis and performance evaluation of heat pipes with multiple heat sources, AIAA/ASME 4th Joint Thermophysics and Heat Transfer Conf. (1986).

ANALYSE DE L'ECOULEMENT DE VAPEUR ET DE LA CONDUCTION THERMIQUE A TRAVERS LA MECHE ET LA PAROI DU TUBE D'UN CALODUC AVEC UNE SEULE OU PLUSIEURS SOURCES DE CHALEUR

Résumé—On présente une analyse numérique pour le comportement global de caloducs avec une seule ou plusieurs sources. L'analyse inclut la conduction thermique dans la paroi et la région liquide-mèche, et aussi l'effet de compressibilité de la vapeur dans le caloduc. Les équations bidimensionnelles elliptiques du problème, avec la relation d'équilibre thermodynamique et les conditions aux limites appropriées sont résolues numériquement. Les solutions sont en accord avec les données expérimentales existantes pour les températures de vapeur et de paroi aussi bien dans le cas de fonctionnement à basse ou haute température.

ANALYSE DER DAMPFSTRÖMUNG UND DER WÄRMELEITUNG DURCH DIE FLÜSSIGKEIT, DEN DOCHT UND DIE ROHRWAND IN EINEM WÄRMEROHR MIT EINZELNEN ODER MEHREREN WÄRMEQUELLEN

Zusammenfassung—Es wird eine numerische Untersuchung für das Gesamtverhalten von Wärmerohren mit einzelnen oder mehreren Wärmequellen vorgestellt. Dabei wird die Wärmeleitung in der Wand und in Flüssigkeits-Dochtgebieten berücksichtigt, ebenso die Kompressibilität im Dampfraum. Die zweidimensionalen elliptischen Bilanzgleichungen werden zusammen mit der Beziehung für das thermodynamische Gleichgewicht und die entsprechenden Randbedingungen numerisch gelöst. Die Lösungen stimmen mit vorhandenen Versuchsdaten für die Dampf- und Wandtemperaturen sowohl bei niedrigen als auch bei hohen Betriebstemperaturen überein.

АНАЛИЗ ТЕЧЕНИЯ ПАРА И ТЕПЛОПРОВОДНОСТИ ЧЕРЕЗ ЖИДКОСТЬ, ФИТИЛЬ И СТЕНКУ В ТЕПЛОВОЙ ТРУБЕ С ЕДИНИЧНЫМ ИЛИ МНОГОЧИСЛЕННЫМИ ИСТОЧНИКАМИ ТЕПЛА

Аннотация—Численно анализируются общие рабочие характеристики тепловых труб с единичным или многочисленными источиками тепла. Наряду с эффектом сжимаемости пара внутри тепловой трубы анализ включает теплопроводность стенки и фитиля с жидкостью. Численно решаются двумерные эллиптические определяющие уравнения совместно с соотношением термодинамического равновесия и соответствующими граничными условиями. Полученные решения согласуются с имеющимися экспериментальными данными для температур пара и стенки как при низких, так и при высоких рабочих температурах.